Journal of Computational Physics 231 (2012) 2389–2395

Contents lists available at SciVerse ScienceDirect

Journal of Computational Physics

journal homepage: www.elsevier.com/locate/jcp

Short note

Stable and accurate integral equation methods for scattering problems with multiple material interfaces in two dimensions

Leslie Greengard, June-Yub Lee *

Courant Institute, New York University, New York, NY 10012, United States

ARTICLE INFO

Article history:
Received 12 August 2011
Received in revised form 14 November 2011
Accepted 23 November 2011
Available online 9 December 2011

Keywords:
Acoustic scattering
Electromagnetic scattering
Triple junctions
Multiple material interfaces
Boundary integral equations

1. Introduction

A number of problems in computational physics require the solution of the Helmholtz equation in domains where multiple media meet at a single point. Examples include acoustic and electromagnetic scattering from structures such as diffraction gratings and complex antennas [6,8,22,25,26].

The geometry of a typical scattering problem is shown in Fig. 1.

We assume that the Helmholtz parameter $k(\mathbf{x})$ is constant in each of the subdomains Ω_0–Ω_4 and that our task is to solve

$$\nabla^2 \Phi^{tot}(\mathbf{x}) + k^2(\mathbf{x})\Phi^{tot}(\mathbf{x}) = 0 \quad \text{for } \mathbf{x} \in R^2, \tag{1}$$

where

$$\Phi^{tot}(\mathbf{x}) = \Phi^{in}(\mathbf{x}) + \Phi(\mathbf{x}), \tag{2}$$

$\Phi^{in}(\mathbf{x})$ is a known incoming field, and $\Phi(\mathbf{x})$ is an unknown scattered field. At material interfaces,

$$\left[\frac{1}{\beta}\Phi^{tot}\right] = 0 \Rightarrow \left[\frac{1}{\beta}\Phi\right] = -\left[\frac{1}{\beta}\Phi^{in}\right] \tag{3}$$

$$\left[\frac{1}{\gamma}\frac{\partial \Phi^{tot}}{\partial \nu}\right] = 0 \Rightarrow \left[\frac{1}{\gamma}\frac{\partial \Phi}{\partial \nu}\right] = -\left[\frac{1}{\gamma}\frac{\partial \Phi^{in}}{\partial \nu}\right] \tag{4}$$

where ν denotes the normal direction, $[f]$ denotes the jump in the quantity f across an interface, and the choice of (β,γ) is determined by the governing physical model.

* Corresponding author. Permanent address: Department of Mathematics, Ewha Womans University, Seoul 120-750, Korea.
E-mail addresses: greengard@cims.nyu.edu (L. Greengard), jyllee@ewha.ac.kr (J.-Y. Lee).

0021-9991/$ - see front matter
doi:10.1016/j.jcp.2011.11.034

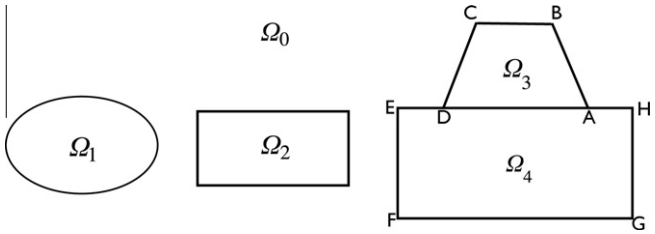

Fig. 1. A progression of singular geometries. We will consider smooth inclusions (left), then corners (center) and finally triple points (right). Triple points are points where three different materials meet, such as *A*, *D*.

In electromagnetics, $k(\mathbf{x}) = \omega\sqrt{\epsilon\mu}$, where ϵ and μ are the permittivity and permeability, respectively, with ω the frequency of interest. In the two-dimensional setting there are two scalar partial differential equations which arise [7,17]. If Φ is the (out-of-plane) z-component of the electric field, then the standard continuity conditions on the tangential components of the electric field require that $\beta = \gamma = 1$ in (3), (4). If Φ is the (out-of-plane) z-component of the magnetic field, then the continuity conditions require that $\beta = 1$, $\gamma = \epsilon$. The latter set of conditions also applies to acoustics with Φ denoting the pressure, in which case $\beta = 1$ and γ is the fluid density. For simplicity of presentation, we will assume $\beta = 1$, since the difficulties we address below stems from the continuity condition (4) on the normal derivative.

In the general case, we assume that the plane $\mathbf{R}^2$ consists of an exterior region Ω_0 in which are embedded some number M of subdomains $\Omega_i, i = 1,\ldots,M$. We will progress through successively more singular problems, beginning with smooth inclusions, then adding corners, and finally triple points (as shown in Fig. 1). The boundary of the i-th domain will be denoted by $\partial\Omega_i$ for $i = 0,\ldots,M$. The total interface will be denoted by $\partial\Omega = \cup_{i=0}^{M}\partial\Omega_i$.

We will restrict our attention here to boundary integral equation approaches since they require a discretization of the interface alone and satisfy the exact Sommerfeld radiation condition for the scattered field. In this short note, we do not seek to review the background potential theory, referring to the texts [11,19,21].

The relevant integral operators are the single and double layer potentials S_k, D_k with source densities σ, μ defined on some (piecewise-smooth) boundary curve Γ:

$$S_k(\Gamma,\sigma,\mathbf{x}) = \int_\Gamma G_k(\|\mathbf{x}-\mathbf{y}\|)\sigma(\mathbf{y})ds_{\mathbf{y}}, \quad D_k(\Gamma,\mu,\mathbf{x}) = \int_\Gamma \frac{\partial G_k}{\partial \nu_{\mathbf{y}}}(\|\mathbf{x}-\mathbf{y}\|)\mu(\mathbf{y})ds_{\mathbf{y}}. \tag{5}$$

We will also require the normal derivatives of S_k and D_k at a point $\mathbf{x} \in \Gamma$.

$$S_k'(\Gamma,\sigma,\mathbf{x}) = \int_\Gamma \frac{\partial G_k}{\partial \nu_{\mathbf{x}}}(\|\mathbf{x}-\mathbf{y}\|)\sigma(\mathbf{y})ds_{\mathbf{y}}, \quad D_k'(\Gamma,\mu,\mathbf{x}) = \int_\Gamma \frac{\partial^2 G_k}{\partial \nu_{\mathbf{x}}\partial \nu_{\mathbf{y}}}(\|\mathbf{x}-\mathbf{y}\|)\mu(\mathbf{y})ds_{\mathbf{y}}. \tag{6}$$

Here, $G_k(r) = \frac{1}{4i}H_0(kr)$ is the Green's function for the Helmholtz equation that satisfies the outgoing radiation condition, where H_0 denotes the Hankel function of the first kind. S_k is weakly singular as $\mathbf{x} \to \Gamma$, and the integral is well-defined. The limiting value of D_k depends on the side of Γ from which $\mathbf{x}$ approaches the curve. For $\mathbf{x} \in \Gamma$, we assume D_k is defined in the principal value sense. Note that S_k' is the adjoint of D_k and should also be interpreted in a principal value sense. The operator D_k', on the other hand, is *hypersingular* and unbounded as a map from the space of smooth functions on Γ to itself. It should be interpreted in the Hadamard finite part sense.

For reasons that will become clear below, we will investigate three possible representations of the scattered field Φ in subdomain Ω_i:

$$(A)\ \Phi_i(\mathbf{x}) = S_{k_i}(\partial\Omega_i,\sigma_i,\mathbf{x}) \tag{7}$$

$$(B)\ \Phi_i(\mathbf{x}) = S_{k_i}(\partial\Omega_i,\sigma,\mathbf{x}) + \gamma_i D_{k_i}(\partial\Omega_i,\mu,\mathbf{x}) \tag{8}$$

$$(C)\ \Phi_i(\mathbf{x}) = S_{k_i}(\partial\Omega,\sigma,\mathbf{x}) + \gamma_i D_{k_i}(\partial\Omega,\mu,\mathbf{x}). \tag{9}$$

A few words of explanation are in order. In (*A*), we assume each (nonsingular) boundary point $\mathbf{y}$ lies at the interface of two subdomains, say Ω_{i_-} and Ω_{i_+} and that it supports two unknown density values: a "charge" density σ_{i_-} which is used to represent the field in Ω_{i_-} and a "charge" density σ_{i_+} which is used to represent the field in Ω_{i_+}. In (*B*), we assume each (nonsingular) boundary point supports an unknown "charge" density σ and an unknown "dipole" density μ which are used to represent the field in both domains Ω_{i_-} and Ω_{i_+} for which $\mathbf{y}$ is a boundary point. In (*C*), the densities $\sigma(\mathbf{y})$, $\mu(\mathbf{y})$ are used to represent the field in *every* subdomain, whether $\mathbf{y}$ is on the boundary of that region or not. This difference will turn out to be essential.

2. The classical integral equations and their discretization

Each of our representations leads to an integral equation. For $\mathbf{x} \in \partial\Omega$, we assume the normal vector $\nu_{\mathbf{x}}$ points from region Ω_{i_-} to region Ω_{i_+}. Substituting the representation (*A*) in (7) into the interface conditions yields the system of integral equations

$$S_{k_{i_+}}(\partial\Omega_{i_+},\sigma_{i_+},\mathbf{x}) - S_{k_{i_-}}(\partial\Omega_{i_-},\sigma_{i_-},\mathbf{x}) = -[\Phi^{in}(\mathbf{x})] \tag{10a}$$

$$-\frac{\sigma_{i_+}(\mathbf{x})}{2\gamma_{i_+}} - \frac{\sigma_{i_-}(\mathbf{x})}{2\gamma_{i_-}} + \frac{1}{\gamma_{i_+}} S'_{k_{i_+}}(\partial\Omega_{i_+},\sigma_{i_+},\mathbf{x}) - \frac{1}{\gamma_{i_-}} S'_{k_{i_-}}(\partial\Omega_{i_-},\sigma_{i_-},\mathbf{x}) = -\left[\frac{1}{\gamma}\frac{\partial\Phi^{in}}{\partial v}(\mathbf{x})\right] \tag{10b}$$

for the unknowns $[\sigma_0,\sigma_1,\ldots,\sigma_M]$.

Substituting the representation (B) in (8) into the interface conditions and taking the appropriate limits yields the system of integral equations

$$\left(\frac{\gamma_{i_+}}{2}+\frac{\gamma_{i_-}}{2}\right)\mu(\mathbf{x}) + S_{k_{i_+}}(\partial\Omega_{i_+},\sigma,\mathbf{x}) - S_{k_{i_-}}(\partial\Omega_{i_-},\sigma,\mathbf{x}) + \gamma_{i_+} D_{k_{i_+}}(\partial\Omega_{i_+},\mu,\mathbf{x}) - \gamma_{i_-} D_{k_{i_-}}(\partial\Omega_{i_-},\mu,\mathbf{x}) = -[\Phi^{in}(\mathbf{x})] \tag{11a}$$

$$\left(-\frac{1}{2\gamma_{i_+}} - \frac{1}{2\gamma_{i_-}}\right)\sigma(\mathbf{x}) + \frac{1}{\gamma_{i_+}} S'_{k_{i_+}}(\partial\Omega_{i_+},\sigma,\mathbf{x}) - \frac{1}{\gamma_{i_-}} S'_{k_{i_-}}(\partial\Omega_{i_-},\sigma,\mathbf{x}) + D'_{k_{i_+}}(\partial\Omega_{i_+},\mu,\mathbf{x}) - D'_{k_{i_-}}(\partial\Omega_{i_-},\mu,\mathbf{x})$$
$$= -\left[\frac{1}{\gamma}\frac{\partial\Phi^{in}}{\partial v}(\mathbf{x})\right] \tag{11b}$$

for the unknowns $[\sigma,\mu]$.

The Eqs. (10a), (10b) form a mixed system of first and second kind Fredholm equations, which are reasonably effective for smooth domains, although the formal theory of existence and uniqueness is not trivial. We will study their performance in Section 4.

The Eqs. (11a), (11b) are a bit more involved. The important aspect of the equations is that, while D' itself is hypersingular, the difference of hypersingular kernels

$$D'_{k_{i_+}}(\partial\Omega_{i_+},\mu,\mathbf{x}) - D'_{k_{i_-}}(\partial\Omega_{i_-},\mu,\mathbf{x})$$

yields a compact operator on smooth domains. In the absence of multi–material junctions, it is only such *difference kernels* that appear in the Eqs. (11a), (11b). As a result, they form a system of Fredholm equations of the second kind, for which the formal theory is classical [12,19] and the solution is easily shown to be unique. The idea of using the difference of hypersingular terms in this manner is standard in electromagnetics [20], acoustics [23], and photonics [13]. We will refer to it as the Müller/Rokhlin scheme, following [20,23].

On smooth domains, major progress has been made in quadrature over the last two decades so that high order accuracy is straightforward to achieve [1,3,18]. The generalized Gaussian quadrature method of [3], in particular, permits the use of composite quadrature rules that take into account the singularity of the Green's function. With K points per subinterval, they achieve K-th order accuracy. In domains with corners (but no multi-material junctions), high-order accurate quadratures that employ exponentially adaptive grids have also been developed, such as [5,15]. (The corner point itself is not part of the discretization.) The basic idea is illustrated in Fig. 2. In the simplest case, suppose that each (piecewise smooth) boundary segment has been subdivided into equal size subintervals of length, say D with a K-th order generalized Gaussian quadrature used on each. The first and last subintervals are the ones that impinge on a corner point, and only these are subdivided using a dyadically refined mesh creating $\log_2\epsilon$ additional subintervals. The same K-th order rule is used on the refined subintervals as well. It is straightforward to show that the resulting rule is "spectrally accurate" in K, with an accumulation of error from each of the $\log_2\epsilon$ refined subintervals, so that the net error is of the order $O(e^{-K}\log_2\epsilon)$. It is, perhaps, worth noting that the purpose of dyadic refinement is simply to resolve the densities σ or μ which develop singularities at the corner points. For $\epsilon = 10^{-14}$ and $K = 16$, the net corner error is about 10^{-14}. For $K = 8$, it is about 10^{-8}. High-order accuracy can also be obtained through the careful use of asymptotic expansions [2].

Remark 2.1. Bremer [4] and Helsing [14] have shown both theoretically and experimentally that the condition number of a properly discretized system of equations is very well controlled and that large scale problems in singular geometries are easily handled by coupling iterative solution methods such as GMRES [24] with these high order discretization and fast multipole acceleration. The formal analysis is more complicated since operators that are compact on smooth domains are not compact (but bounded) on domains with corners. Part of the point of [4,14] is that when carefully discretized, the level of difficulty is not, in fact, much greater.

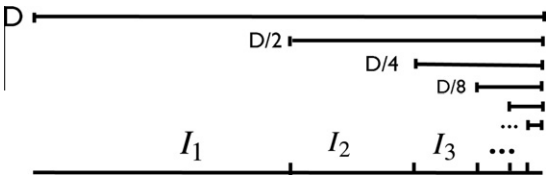

Fig. 2. For geometric singularities, we use a progression of dyadic intervals to discretize the unknown charge/dipole densities on each boundary segment that meets at the singular point. Each dyadically refined interval is separated from the endpoint by its length.

Remark 2.2. Related recent work [5,15] has shown that one can dramatically reduce the number of degrees of freedom in the vicinity of the corner by the use of *compression*. We are primarily interested here in robustness and accuracy (rather than speed) and omit any discussion of either compression or fast algorithms in the present note.

3. Extending the Müller/Rokhlin scheme to multi-material junctions

In the case of triple junctions, the Eqs. (11a), (11b) fail to converge. The reason for this is simple. Consider the interface condition (10b) for $\mathbf{x}$ lying on the segment $\overline{CD}$ in Fig. 1. Writing out the detailed contributions from just the segments impinging on the corner point D, we have

$$\left(-\frac{1}{2\gamma_0}-\frac{1}{2\gamma_4}\right)\sigma(\mathbf{x})+\left[\frac{1}{\gamma_0}S'_{k_0}(\overline{CD},\sigma,\mathbf{x})-\frac{1}{\gamma_4}S'_{k_4}(\overline{CD},\sigma,\mathbf{x})\right]+\frac{1}{\gamma_0}S'_{k_0}(\overline{DE},\sigma,\mathbf{x})-\frac{1}{\gamma_4}S'_{k_4}(\overline{DA},\sigma,\mathbf{x})+\cdots$$
$$+\left[D'_{k_0}(\overline{CD},\mu,\mathbf{x})-D'_{k_4}(\overline{CD},\mu,\mathbf{x})\right]+D'_{k_0}(\overline{DE},\mu,\mathbf{x})-D'_{k_4}(\overline{DA},\mu,\mathbf{x})+\cdots=-\left[\frac{1}{\gamma}\frac{\partial\Phi^{in}}{\partial\nu}(\mathbf{x})\right] \tag{12}$$

Both the terms $D'_{k_0}(\overline{DE},\mu,\mathbf{x})$ and $D'_{k_4}(\overline{DA},\mu,\mathbf{x})$ involve hypersingular contributions at the junction D without forming part of a difference kernel. As we shall see, this destroys the high-order accuracy of the scheme.

By using the global integral representation (C) in (9), we eliminate such terms from the integral equation. Only difference kernels appear in the resulting system. For $\mathbf{x}\in\partial R$, we have

$$\left(\frac{\gamma_{i_+}}{2}+\frac{\gamma_{i_-}}{2}\right)\mu(\mathbf{x})+S_{k_{i_+}}(\partial\Omega,\sigma,\mathbf{x})-S_{k_{i_-}}(\partial\Omega,\sigma,\mathbf{x})+\gamma_{i_+}D_{k_{i_+}}(\partial\Omega,\mu,\mathbf{x})-\gamma_{i_-}D_{k_{i_-}}(\partial\Omega,\mu,\mathbf{x})=-[\Phi^{in}(\mathbf{x})] \tag{13a}$$

$$\left(-\frac{1}{2\gamma_{i_+}}-\frac{1}{2\gamma_{i_-}}\right)\sigma(\mathbf{x})+\frac{1}{\gamma_{i_+}}S'_{k_{i_+}}(\partial\Omega,\sigma,\mathbf{x})-\frac{1}{\gamma_{i_-}}S'_{k_{i_-}}(\partial\Omega,\sigma,\mathbf{x})+D'_{k_{i_+}}(\partial\Omega,\mu,\mathbf{x})-D'_{k_{i_-}}(\partial\Omega,\mu,\mathbf{x})=-\left[\frac{1}{\gamma}\frac{\partial\Phi^{in}}{\partial\nu}(\mathbf{x})\right] \tag{13b}$$

Remark 3.1. Recently, several groups have addressed the issue of deriving well-conditioned integral equations for multi-material junctions using Dirichlet and Neumann data as unknowns rather than abstract layer potentials. In [16], a first kind equation was derived that is suitable for Calderon-type preconditioning, and in [9,10] a second kind equation was derived and shown to be effective without preconditioning.

4. Numerical results

The algorithms discussed above have been implemented in Fortran, using 8th order generalized Gaussian quadrature rules [3]. For discretization, we divide each boundary segment (in the piecewise smooth boundary) into M equal subintervals. The first and last intervals are subdivided dyadically into M_{dyadic} subintervals. As a result, the total number of points on each boundary segment (each side) is $8\cdot(M-2)+16\cdot M_{dyadic}$. The corner truncation error from dyadic refinement (when the scheme is convergent) is approximately $2^{-M_{dyadic}}$. We solve the integral Eqs. (10a), (10b), (11a), (11b), (13a), (13b) iteratively using GMRES with a tolerance of 10^{-8}.

Example 1 (*Comparing representations (A) and (B)*). In the first example (Fig. 3), we consider a domain with corners but no triple points. $\omega=1$ with $\epsilon=1$, $k=1$ in the exterior region and $\epsilon=20$, $k=10$ in the inclusion. The incoming field is defined to be a plane wave at incident angle 120° with respect to the $+x$-axis. The object is approximately two wavelengths in size (in

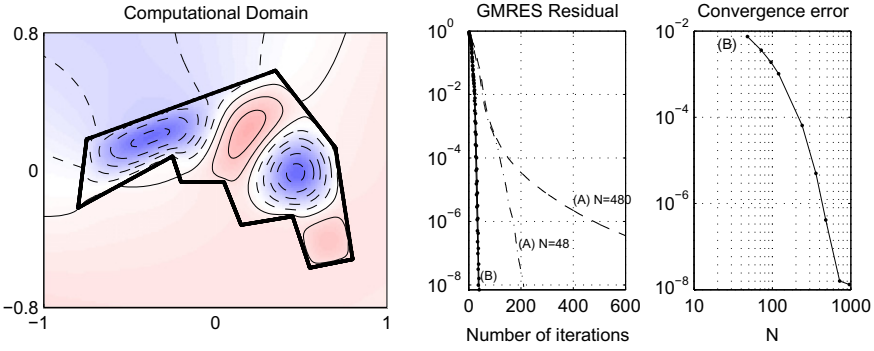

Fig. 3. A domain with corners: the geometry and solution are shown on the left and the convergence rate of GMRES is shown in the center. The right-hand plot shows the error in the solution as a function of the number of discretization points using representation (B).

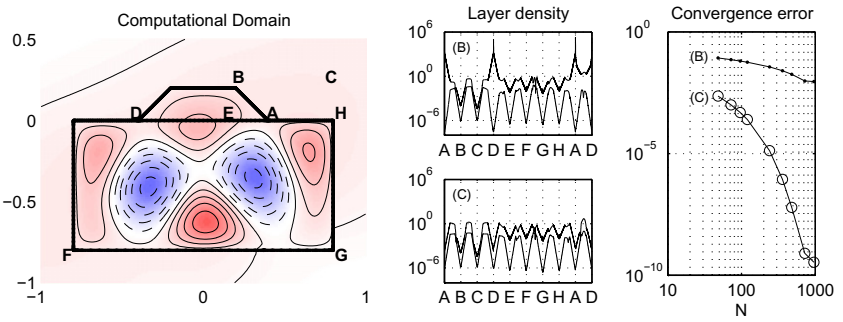

Fig. 4. Comparison of representations (*B*) and (*C*) for domains with triple points. (See text for explanation.)

terms of the interior Helmholtz parameter). The left-hand plot shows $Re[\Phi^{tot}]$. The central plot shows the behavior of GMRES (residual vs. iteration number) using representations (*A*) and (*B*) with either $M = 22$, $M_{dyadic} = 20$ which corresponds to $N = 480$ points per side or $M = 4$, $M_{dyadic} = 2$ which corresponds to $N = 48$ points per side. The integral Eqs. (11a), (11b) from representation (*B*) required 40 iterations, yielding the rapidly converging curve (solid line with superimposed dots). The integral Eqs. (10a), (10b) from representation (*A*) yields the dash-dotted curve for $N = 48$ and the dashed curve for $N = 960$. 211 iterations were required in the former case, and more than 1200 iterations in the latter. Note that the second kind equation from representation (*B*) is well conditioned (from the GMRES behavior) and high order accurate (from the right-hand plot). Moreover, there is no loss of precision from overresolution.

Example 2 (*Comparing representations (B) and (C)*). Since the representation (*A*) leading to a mixed system of first and second kind equations has been shown not to be robust when simple corners are present, we compare only representations (*B*) and (*C*) in the presence of triple points. In Fig. 4, we again set $\omega = 1$, with $\epsilon = 1$, $k = 1$ in the exterior region, $\epsilon = 9$, $k = 6$ in the trapezoidal subdomain, and $\epsilon = 20$, $k = 10$ in the rectangular subdomain (shown in the left-hand plot). The incoming field is a plane wave at incident angle 120° with respect to the $+x$-axis. On the left, we also plot $Re[\Phi^{tot}]$. The central plot shows the solution to the integral equation as one traverses the boundary $\partial\Omega$ from vertex to vertex in the indicated order. The upper curves in each plot show the single layer density σ and the lower curves in each plot the double layer density μ. The top center figure correspond to representation (*B*) and the bottom center figure to representation (*C*). Note the singular behavior of σ at the triple junctions in the former case and the well-behaved nature of the solution in the latter case (the solution is still weakly singular but no longer diverges.)

The right-hand plot shows the error in using representations (*B*) (upper curve) and (*C*) (lower curve) as the number of discretization points is increased. Representation (*C*) behaves just like the classical approach on domains with corners but no triple points. When using representation (*C*), only 38–42 iterations were required for each value of *N* indicated. For representation (*B*), the iteration count grew with *N* from 37 to 117 in order to achieve a residual of 10^{-8}. The actual error is visibly much worse.

Example 3 (*High contrast case*). Our final example involves a more difficult problem, with a dielectric contrast of 10^4. The computational domain is shown at the left of Fig. 5 with $(\epsilon_i, k_i) = (1, 10), (8, 40)$ and $(10^4, 10^3)$ in the exterior, the large circle and the small circle, respectively. The incoming field is a plane wave at incident angle 120° with respect to the $+x$-axis. Not only is there a large impedance mismatch between the small circle and the two other subdomains, the Helmholtz coefficient is so large that the circle is about 100 wavelengths across, and it functions as a nearly resonant cavity. The image is marked `void` on the left and in the center, because the wavelength is so small it is below the available resolution. The center figure is a zoom in on the rectangle indicated in the left-hand figure. Zooming in again on the rectangle shown in the center figure

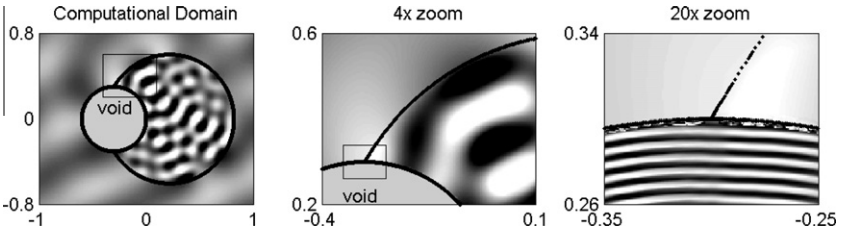

Fig. 5. A high frequency, high contrast, scattering calculation with triple points. (See text for explanation.)

yields the image on the right. At that scale, the wavelength is large enough to be visible. It is important to note that 700 GMRES iterations were required to achieve a tolerance of 10^{-9} here, and that the solution was correct to between 6 and 7 digits, with $M = 180$ and $M_{dyadic} = 30$. Both the iteration count and the loss of 2–3 digits in accuracy are to be expected, since the condition number of the physical problem grows linearly with k.

Remark 4.1. We have used a simple and robust test for estimating the accuracy of each method. Rather than solve the true scattering problem, we can define interior and exterior fields due to fictitious sources. That is, for $\mathbf{x} \in \Omega_i$, we assume the field is due to known sources located in each of the other domains. These sources give rise to fields with artificial jumps in $\frac{1}{\beta}\Phi, \frac{1}{\gamma}\frac{\partial \Phi}{\partial \nu}$ and we can solve for σ, μ to annihilate those jumps. The fields induced by σ, μ can then be compared to the known analytic solution at any target. We have also used standard self-consistent error estimation. Both approaches yield errors of the magnitude listed above.

5. Conclusions

We have described a simple modification of the classical Müller/Rokhlin integral equation for the calculation of scattering from composite structures with multi-material junctions. The resulting linear system is well-conditioned and the combination of high-order quadratures for smooth densities with adaptive corner refinement yields rapid convergence. The novel feature of our scheme is the use of *all* boundary components to represent the field in each subdomain, rather than just the boundary of the subdomain itself. One could improve efficiency somewhat, while achieving similar results, by using representation (B) for each subdomain, supplemented only by the boundary segments that happen to impinge on any multi-material junction points that are present. We have used the fully global representation in our experiments above for the sake of simplicity.

Extension of our method to three dimensions and to the elastic and full electromagnetic cases are underway, as is the coupling of the scheme to suitable fast algorithms. These developments will be reported at a later date.

Acknowledgements

This work was supported in part by the Applied Mathematical Sciences Program of the U.S. Department of Energy under Contract DEFGO288ER25053 and by the Air Force Office of Scientific Research under MURI grant FA9550-06-1-0337 and under NSSEFF Program Award FA9550-10-1-0180. JYL was also supported in part by the Priority Research Centers Program from National Research Foundation of Korea, NRF-2010-0028298.

References

[1] B.K. Alpert, Hybrid Gauss-trapezoidal quadrature rules, SIAM J. Sci. Comput. 20 (1999) 1551–1584.
[2] A.H. Barnett, T. Betcke, An exponentially convergent nonpolynomial finite element method for time-harmonic scattering from polygons, SIAM J. Sci. Comput. 32 (2010) 1417–1441.
[3] J. Bremer, Z. Gimbutas, V. Rokhlin, A nonlinear optimization procedure for generalized Gaussian quadrature, SIAM J. Sci. Comput. 32 (2010) 1761–1788.
[4] J. Bremer, "On the Nyström discretization of integral equations on planar curves with corners", Appl. Comput. Harm. Anal. (2011), doi:10.1016/j.acha.2011.03.002.
[5] J. Bremer, V. Rokhlin, V. Sammis, Universal quadratures for boundary integral equations on two-dimensional domains with corners, J. Comput. Phys. 229 (2011) 8259–8280.
[6] M.E. Carr, E. Topsakal, J.L. Volakis, A procedure for modeling material junctions in 3-D surface integral equation approaches, IEEE Trans. Antennas Propag. 52 (2004) 374–1379.
[7] W.C. Chew (Ed.), Waves and Fields in Inhomogeneous Media, IEEE Press House, New York, 1995.
[8] W.C. Chew, J.-M. Jin, E. Michielssen, J. Song, Fast and Efficient Algorithms in Computational Electromagnetics, Artech House, Boston, 2001.
[9] X. Claeys, A single trace integral formulation of the second kind for acoustic scattering, in: ETH, Seminar of Applied Mathematics Research, 2011, Report no. 2011-14.
[10] X. Claeys, Integral formulation of the second kind for multi-subdomain scattering, in: Proceedings 10th International Conference on Mathematics Numerical Aspects of Waves (WAVES 2011), Pacific Institute for the Mathematical Sciences, pp. 129–132 (http://www.pims.math.ca/).
[11] D. Colton, R. Kress, Integral Equation Methods in Scattering Theory, Wiley, New York, 1983.
[12] R.B. Guenther, J.W. Lee, Partial Differential Equations of Mathematical Physics and Integral Equations, Prentice-Hall, Englewood Cliffs, New Jersey, 1988.
[13] M.A. Haider, S.P. Shipman, S. Venakides, Boundary-integral calculations of two-dimensional electromagnetic scattering in infinite photonic crystal slabs: channel defects and resonances, SIAM J. Appl. Math. 62 (2002) 2129–2148.
[14] J. Helsing, The effective conductivity of random checkerboards, J. Comput. Phys. 230 (2011) 1171–1181.
[15] J. Helsing, R. Olaja, Corner singularities for elliptic problems: integral equations, graded meshes, and compressed inverse preconditioning, J. Comput. Phys. 227 (2008) 8820–8840.
[16] R. Hiptmair, C. Jerez-Hanckes, Multiple traces boundary integral formulation for Helmholtz transmission problems, in: ETH, Seminar of Applied Mathematics Research Report no. 2010-30.
[17] J.D. Jackson, Classical Electrodynamics, Wiley, New York, 1975.
[18] R. Kress, Boundary integral equations in time-harmonic acoustic scattering, Math. Comput. Model. 15 (1991) 229–243.
[19] S.G. Mikhlin, Integral Equations, Pergammon Press, London, 1957.
[20] C. Müller, Foundations of the Mathematical Theory of Electromagnetic Waves, Springer-Verlag, Berlin, New York, 1969.
[21] J.-C. Nédélec, Acoustic and Electromagnetic Equations, Springer-Verlag, New York, 2001.
[22] J.M. Putnam, L.N. Medgyesi-Mitschang, Combined field integral equation for inhomogeneous two – and three-dimensional bodies: the junction problem, IEEE Trans. Antennas Propag. 39 (1991) 667–672.

[23] V. Rokhlin, Solution of acoustic scattering problems by means of second kind integral equations, Wave Motion 5 (1983) 257–272.
[24] Y. Saad, M.H. Schultz, GMRES: a generalized minimum residual algorithm for solving nonsymmetric linear systems, SIAM J. Sci. Stat. Comput. 7 (1986) 856–869.
[25] M.S. Yeung, Single integral equation for diffraction from dielectric gratings in layered media, Microwave Opt. Tech. Lett. 32 (2002) 383–388.
[26] P. Yla-Oijala, M. Taskinen, J. Sarvas, Surface integral equation method for general composite metallic and dielectric structures with junctions, Prog. Electromag. Res. PIER 52 (2005) 81–108.